ISSN 1063-7826, Semiconductors, 2017, Vol. 51, No. 1, pp. 122–130. © Pleiades Publishing, Ltd., 2017.
Original Russian Text © P.V. Seredin, A.S. Lenshin, I.N. Arsentiev, A.V. Zhabotinskii, D.N. Nikolaev, I.S. Tarasov, V.V. Shamakhov, Tatiana Prutskij, Harald Leiste, Monika Rinke, 2017, published in Fizika i Tekhnika Poluprovodnikov, 2017, Vol. 51, No. 1, pp. 124–132.

FABRICATION, TREATMENT, AND TESTING OF MATERIALS AND STRUCTURES

Epitaxial $Al_xGa_{1-x}As$:Mg Alloys with Different Conductivity Types

P. V. Seredin[a]*, A. S. Lenshin[a], I. N. Arsentiev[b], A. V. Zhabotinskii[b], D. N. Nikolaev[b], I. S. Tarasov[b], V. V. Shamakhov[b], Tatiana Prutskij[c]***, Harald Leiste[d], and Monika Rinke[d]**

[a] *Voronezh State University, Voronezh, 394006 Russia*
[b] *Ioffe Physical–Technical Institute, Russian Academy of Sciences, St. Petersburg, 194021 Russia*
[c] *Instituto de Ciencias, Benemérita Universidad Autónoma de Puebla, Puebla, 72050 Mexico*
[d] *Karlsruhe Nano Micro Facility, Eggenstein-Leopoldshafen, 76344 Germany*
*e-mail: *paul@phys.vsu.ru, **arsentyev@mail.ioffe.ru, ***prutskiy@yahoo.com*

Submitted June 2, 2016; accepted for publication June 14, 2016

Abstract—The structural, optical, and energy properties of epitaxial $Al_xGa_{1-x}As$:Mg/GaAs(100) heterostructures at different levels of doping with Mg are studied by high-resolution X-ray diffraction analysis and Raman and photoluminescence spectroscopies. It is shown that, by choosing the technological conditions of $Al_xGa_{1-x}As$:Mg alloy production, it is possible to achieve not only different conductivity types, but also substantially different charge-carrier concentrations in an epitaxial film.

DOI: 10.1134/S1063782617010213

1. INTRODUCTION

Progress in the production of semiconductor nanoheterostructures is defined by the demands of high-tech production works for optoelectronic components with new functional characteristics. Therefore, numerous studies on the physics and technology of semiconductor heterostructures are devoted to the methods of their formation by molecular-beam epitaxy and metal–organic chemical vapor deposition [1, 2]. Studies concerned with the systematic features of the doping of epitaxial heterostructures based on Group-III–V compounds are no less important, since highly efficient optoelectronic components based on Group-III–V compounds can only be attained with unambiguous concepts of the structural, optical, and energy properties of the constituent materials of the heteropair and with an understanding of the processes and systematic features of the doping of epitaxial alloys with acceptor and donor impurities. Impurities are introduced into the semiconductor layer to controllably vary the conductivity type as well as a number of electrooptical properties [3–5].

Doping of GaAs and GaAs-based alloys with various impurities is an old problem. Nevertheless, annual growth in the use of GaAs nanoheterostructures in optoelectronic devices is stimulating the search for solutions to old problems and a new look at classical materials [6–11].

The development of new methods of doping [12], including precise monitoring of the level of doping [13] and new methods of impurity reactivation [14, 15], have resulted in considerable improvement in the quality of epitaxial layers and, as a consequence, have extended the field of their application [16, 17]. The main dopant impurities in Group-III–V compounds are carbon and silicon. However, although these impurities are commonly used and their behavior as dopants have been much studied, a number of unsolved problems associated with the potential application of impurities are still facing researchers [10, 18]. These factors are motivating the search for new dopant elements and mechanisms of doping.

Specifically, at present, for the *p*-type dopant in epitaxial GaAs and AlGaAs layers, beryllium (Be) which possesses high incorporation coefficients and a low vapor pressure at standard growth temperatures is used. Nevertheless, because of the high toxicity of Be, researchers are more and more often searching for alternative impurities that are not so toxic and carcinogenic. Among the possible variants, magnesium (Mg) is most promising [19–21]. The use of Mg is rather advantageous, since it exhibits a high solubility in Group-III–V alloys and, when incorporated into cation sites of the alloys, gives a shallow acceptor level [22–25]. In addition, Mg-doped epitaxial layers exhibit a lower resistivity at the same composition in comparison with layers doped with similar impurities serving as *p*-type dopants.

It is known that the charge-carrier mobility and concentration in an $Al_xGa_{1-x}As$ layer doped with Mg heavily depend on the Al molar fraction in the As/Ga ratio.

In studies [26–29] concerned with the growth of $Al_xGa_{1-x}As$ layers containing Mg impurities, it was

Table 1. Technological parameters of growth of $Al_xGa_{1-x}As$:Mg/GaAs(100) heterostructures

Sample	Composition parameter x	T_{growth}, °C	$T_{bubbler}$, °C	Conductivity type and charge-carrier concentration, cm^{-3}	Mg molar flux, mol min^{-1}
EM2916	0.10	700	18	$p = 1.2 \times 10^{15}$	1.3×10^{-8}
EM2918	0.10	700	14	$p = 1.2 \times 10^{17}$	8.8×10^{-9}
EM2921	0.10	700	10	$n = 7.0 \times 10^{14}$	5.8×10^{-9}

shown that the MBE or MOCVD growth of the layers on GaAs(100) substrates yielded a decrease in the charge-carrier concentration in the $Al_xGa_{1-x}As$ layer from 10^{17} to 10^{14} cm^{-3}. This difference between the charge-carrier concentrations was attributed to a sharp decrease in the Mg concentration in Group-III–V epitaxial layers with increasing substrate temperature.

The desire of researchers to fabricate epitaxial layers with the maximum mobility and to grow layers isoperiodic to a single-crystal GaAs(100) substrate, with minimum strains arising from the mismatch between crystal lattices, is an interesting and promising task.

In this context, the purpose of this study is to explore the properties of Mg-doped epitaxial $Al_xGa_{1-x}As$ alloy layers by a set of structural and spectral techniques.

2. EXPERIMENTAL

Epitaxial heterostructures based on $Al_xGa_{1-x}As$:Mg alloys were produced on GaAs(100) substrates by MOCVD epitaxy. Epitaxy was conducted using an Emcore GS 3100 setup at a reduced reactor pressure (0.1 atm) and a high rotational speed of the substrate holder (1000 rpm).

For all of the samples, the alloy composition was set at $Al_{0.103}Ga_{0.897}As$. The layer growth rate was 625 Å min^{-1}, the growth temperature was 700°C, and the layer thickness was 2 μm.

For the Al and Ga sources, we used trimethylaluminun ($Al(CH_3)_3$) and trimethylgallium ($Ga(CH_3)_3$), respectively. The source of Group-V elements was arsine (AsH_3, 100%). To dope the AlGaAs alloys with Mg, the gas-carrier (hydrogen) flow was passed through a bubbler with bis(cyclopentadienyl)magnesium ($Mg(C_5H_5)_2$). The rate of flow through the bubbler was 5 cm^3 min^{-1}. For different samples, the bubbler temperature was varied in the range from 10 to 18°C; the pressure was kept at 0.5 atm. The technological characteristics of the samples are listed in Table 1.

The structural quality of the samples and the lattice parameters of the alloys were determined by the X-ray diffraction (XRD) technique using a Seifert 3003 HR diffractometer with a four-circle goniometer. In the XRD measurements, we used monochromatic Cu$K_{\alpha 1}$ radiation with the wavelength 1.5405 Å.

The content of elements in the alloy was refined by X-ray microanalysis, using a special electron-microscope attachment.

The Raman spectra were obtained with the use of a Renishaw 1000 Raman spectrometer equipped with a microscope with a ×50 NPlan lens. As the excitation source, we used an argon laser emitting at a wavelength of 514.5 nm. The laser-beam power was no higher than 3 mW.

The photoluminescence (PL) spectra of the heterostructures were obtained by detecting the signal from the sample surface at room temperature. The PL measurements were conducted by the standard procedure with a TRIAX550 monochromator equipped with a CCD detector cooled with liquid nitrogen. To excite the PL spectra, we used an argon laser emitting at the wavelength 514.5 nm. The laser beam was focused onto the surface with a 10× lens.

The charge-carrier concentration and conductivity type were determined by Hall measurements at room temperature (see Table 1).

3. RESULTS AND DISCUSSION

3.1. X-Ray Microanalysis

X-ray microanalysis allowed us to refine the content of elements included in the epitaxial films. In the analysis, we used an electron accelerating voltage of 20 kB. We studied sample areas 750 × 750 μm in dimensions. The effective depth of microanalysis was about 0.5 μm.

The results show that the atomic content in the epitaxial film only slightly differs from the content specified in the stage of growth. The experimentally determined composition of the alloys corresponded to $Al_{0.103}Ga_{0.897}As$.

From the measurements of the free-charge-carrier concentration in the epitaxial films at room temperature, it is found that, for the samples grown, the hole concentration in the layer increases, as the bubbler temperature is lowered from 18 to 14°C. As the bubbler temperature is lowered further to 10°C, p-type conductivity changes to n-type.

3.2. High-Resolution XRD

In present-day studies of semiconductor nanoheterostructures, the high-resolution XRD technique

provides a means for solving a number of problems, among which are determination of the parameters of epitaxial structures, refinement of the layer composition, the separation of deformations from misorientations in epitaxial layers, and determination of the degree of relaxation of the crystal-lattice parameters of epitaxial layers to the parameters of substrates in heterostructures [9, 25, 30, 31].

The optimal approach to analyzing the structure and structural changes by XRD methods is the mapping of reciprocal space. This method makes it possible to detect structural defects and compositional or strain gradients in an epitaxial layer by observing changes in the distribution of the diffracted radiation intensity around the lattice site.

It is well known that the crystal-lattice parameters of the epitaxial layer of a heterostructure in the growth direction ($a^{\perp}$) and in the growth plane ($a^{\parallel}$) can be determined from data obtained by analyzing maps of reciprocal q space for the symmetric (400) and asymmetric (511) reflections. Specifically, the parameter $a^{\perp}$ can be determined from data for the symmetric (400) or asymmetric (511) reflections as $q_{400}^{\text{epilayer}} = (h^2/a^{\perp})^{1/2}$ or $q_{500}^{\text{epilayer}} = (h^2/a^{\perp})^{1/2}$, respectively. At the same time, the parameter $a^{\parallel}$ is determined only from the data for the asymmetric (511) reflection by the relation

$$q_{011}^{\text{epilayer}} = \left(\frac{(k^2 + l^2)^2}{a^{\parallel}}\right)^{1/2}.$$

Here q_{500} and q_{011} are the lattice vectors in reciprocal q space.

If we introduce the Poisson coefficient for a cubic crystal ν, the crystal-lattice parameter of the epitaxial film with consideration for internal strains (the parameter is commonly denoted by a^{ν}) can be calculated in accordance with linear elasticity theory:

$$a^{\nu} = a^{\perp}\frac{1-\nu}{1+\nu} + a^{\parallel}\frac{2\nu}{1+\nu}. \quad (1)$$

Since the heterostructure samples are here grown in the region of compositions isoperiodic to the GaAs(100) substrate, we use linear interpolations for Vegard's law, Poisson coefficients, and the compositional dependence of the band gap similarly to how it was done in previous studies [9, 10, 32, 33].

Thus, with consideration for the linear dependence of the Poisson coefficients on the composition parameter x for an epitaxial $Al_xGa_{1-x}As$ film grown on a GaAs substrate,

$$\nu_{A_xB_{1-x}C} = x\nu_{AC} + (1-x)\nu_{BC},$$

expression (1) takes the form

$$\nu^{x}_{A_xGa_{1-x}As} = a^{\perp}_{A_xGa_{1-x}As}\frac{1-(x\times x_{AlAs}+(1-x)x_{GaAs})}{1+(x\times x_{AlAs}+(1-x)x_{GaAs})} + a^{\parallel}_{A_xGa_{1-x}As}\frac{2(x\times x_{AlAs}+(1-x)x_{GaAs})}{1+(x\times x_{AlAs}+(1-x)x_{GaAs})}. \quad (2)$$

Figure 1 shows the maps of the distribution of the diffracted radiation intensity around the site of the reciprocal lattice for the (400) planes (symmetric scan) and for the (511) planes (asymmetric scan) of the samples under study. It can be clearly seen that the distribution of the diffracted-radiation intensities for the symmetric and asymmetric scans presents a single reflection (site). Detailed analysis of the maps of backscattering allowed us to establish that, for all three samples, the reciprocal lattice vectors in the growth plane and, consequently, the lattice parameters of the film and substrate are the same. This means that the epitaxial film grows to match the substrate in terms of lattice parameter. At the same time, as follows from precise consideration of the results of mapping of reciprocal space, the lattice parameter of the epitaxial film in the growth direction differs from the lattice parameter of the single-crystal GaAs substrate.

Table 2 lists the mismatches between the lattice vectors $q^{\perp}$ and $q^{\parallel}$ in reciprocal space, as determined from the (400) and (511) maps. It is found that, for all of the samples, the mismatches in the growth direction of the epitaxial film are equal, which is indicative of the growth of films identical in composition, ideally matched in terms of lattice parameter in the growth plane, and strained, but not compositionally degraded.

From a qualitative analysis of maps of reciprocal space, it is also possible to draw a number of important conclusions. It can be clearly seen (especially for the asymmetric scan) that the shapes of the site in reciprocal space are different for different samples. The broadening of the (511) site in the $q^{\parallel}$ direction (see Figs. 1b, 1d, 1f) is indicative of the presence of defects in the film. The most pronounced broadening of the (511) site is noticed for sample EM2921 which exhibits the lowest charge-carrier concentration and n-type conductivity.

The deviation of the line of interference maxima from the $q^{\perp}$ direction on the map of the (400) site for all of the heterostructure samples suggests that growth occurred on substrates initially misoriented with respect to the (100) direction.

Assuming the validity of Vegard's law for the system of $Al_xGa_{1-x}As$:Mg alloys produced isoperiodic to the GaAs substrate, by analyzing expression (1), calculating the crystal-lattice parameters, and taking into account the data of microanalysis, we determined the refined content of constituent elements of the alloys (Table 2). Table 2 also lists the crystal-lattice parameters determined, with consideration for elastic strains

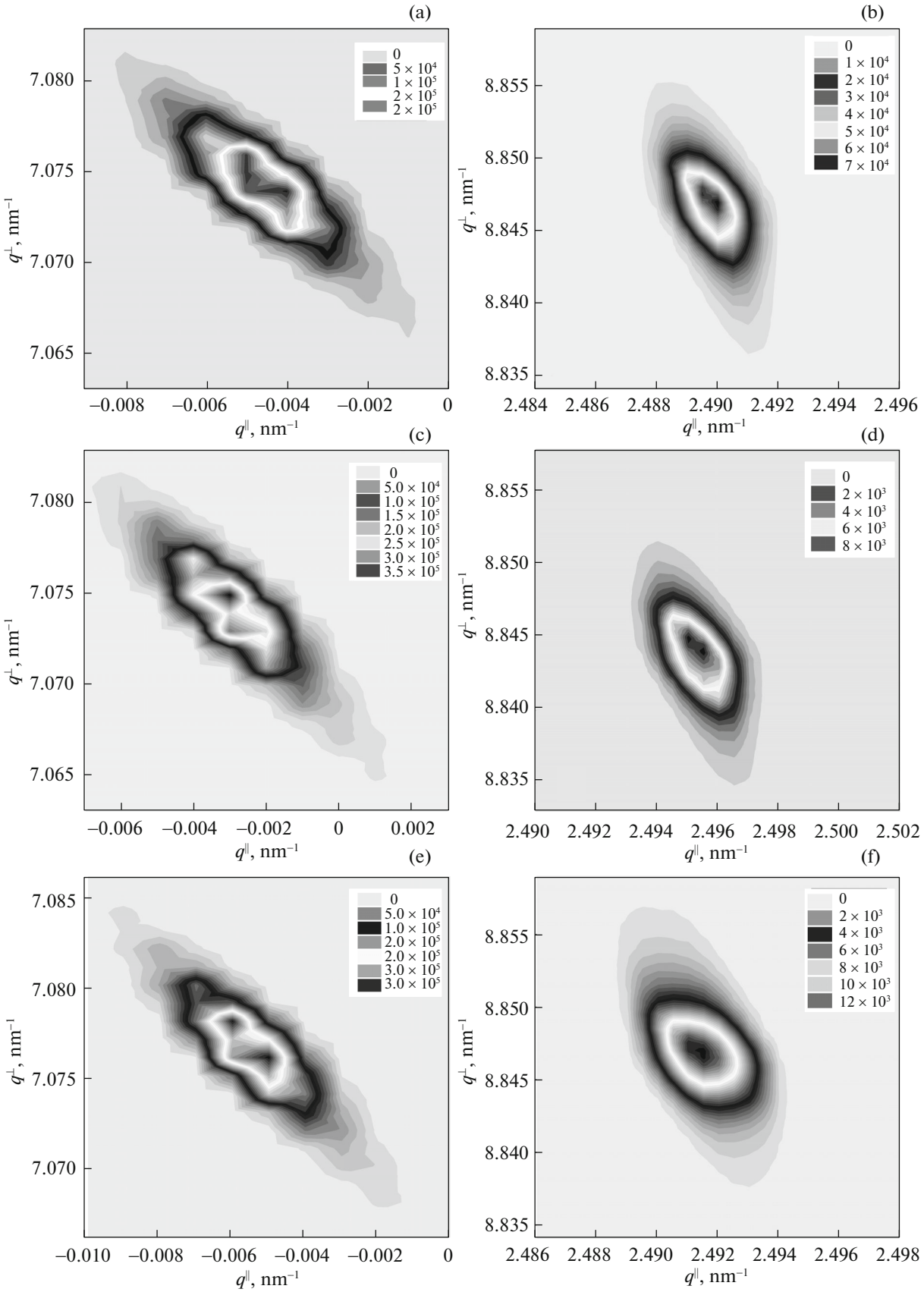

Fig. 1. Maps of reciprocal q space around (left) the (400) and (right) (511) sites for $Al_xGa_{1-x}As$:Mg/GaAs(100) heterostructures (a, b) EM2916, (c, d) EM2918, and (e, f) EM2921.

Table 2. High-resolution XRD data

Sample	Heterostructure component	Reciprocal lattice site				Composition parameter x	Lattice parameter $a^{v\|}$, Å
		(400)		(511)			
		$q^{\perp}$, nm^{-1}	$q^{\|}$, nm^{-1}	$q^{\perp}$, nm^{-1}	$q^{\|}$, nm^{-1}		
		$\Delta q^{\perp}$, nm^{-1}	$\Delta q^{\|}$, nm^{-1}	$\Delta q^{\perp}$, nm^{-1}	$\Delta q^{\|}$, nm^{-1}		
EM2916	GaAs substrate	7.0755	–0.0040	8.8445	2.4900	–	5.6532
	$Al_xGa_{1-x}As$ layer	+0.0020	0	+0.0025	0	0.103	5.6541
EM2918	GaAs substrate	7.0755	–0.0030	8.8440	2.4950	–	5.6532
	$Al_xGa_{1-x}As$ layer	+0.0020	0	+0.0025	0	0.103	5.6541
EM2921	GaAs substrate	7.0760	–0.0050	8.8445	2.4915	–	5.6532
	$Al_xGa_{1-x}As$ layer	+0.0020	0	+0.0025	0	0.103	5.6541

in epitaxial alloys, from experimental data on maps of the scattering intensity in reciprocal space, the data of microanalysis, and Vegard's law.

3.3. Raman Scattering

The effective depth of analysis by Raman spectroscopy can be determined from the relation $\lambda/2\pi k$, where k is the extinction coefficient. Using the argon laser emitting at a wavelength of $\lambda = 532$ nm for the analysis of heterostructures based on $Al_xGa_{1-x}As$ alloys, we established that the penetration depth of the laser radiation and, consequently, the depth of analysis does not exceed 500 nm. Thus, we can state with confidence that, using a laser emitting at the above-indicated wavelength in Raman spectroscopy, we gain information on the layer of the alloy only.

From the analysis of Raman tensors [34], it is well known that, according to the selection rules for structurally diamond-like crystals, only longitudinal optical (LO) phonons can be observed upon backscattering from the (100) surface, whereas the observation of transverse optical (TO) phonons is forbidden.

Figure 2 shows the Raman spectra recorded in the $x(y, z)\bar{x}$ geometry of the experiment for $Al_xGa_{1-x}As$:Mg heterostructures with different levels of doping with Mg. As can be seen from the results, the spectra of the heterostructures exhibit LO_{Ga-As} and LO_{Al-As} phonon modes characteristic of $Al_xGa_{1-x}As$ alloys. From Fig. 2, it can be clearly seen that the LO vibrational frequencies are identical for all samples. This is supported by high-resolution XRD data indicative of the same composition of the alloy in all of the heterostructures.

It should be noted that, in the experimental Raman spectra of all of the heterostructures, there are TO_{Ga-As} and TO_{Al-As} vibration modes forbidden by the selection rules (see the inset in Fig. 2). This is a consequence of violation of the crystal-lattice symmetry of the epitaxial film.

From a more detailed analysis of the Raman data, it is possible to detect an additional low-intensity mode that appears in the spectra of $Al_xGa_{1-x}As$:Mg heterostructures at the frequency $\omega \sim 510$–530 cm^{-1} (against the background of the main vibrations) (see inset in Fig. 2). Analyzing the results and the technological conditions of growth of the heterostructures (Table 1), we can see that the intensity of this phonon mode varies under variations in the Mg source temperature. It would be logical to conceive that this mode can be a consequence of vibrations of the bonds of Mg atoms with their nearest neighbors.

It was possible to confirm these assumptions on the basis of a simple calculation of vibrational frequencies of nearest neighbors in a diamond-like lattice within the context of the model proposed by Harrison [35] and successfully tested in [32, 36].

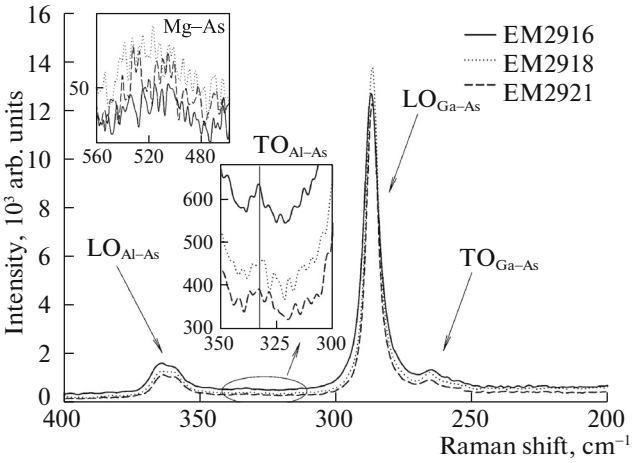

Fig. 2. Raman spectra of $Al_xGa_{1-x}As$:Mg/GaAs(100) heterostructures.

Table 3. PL spectroscopy data for $Al_xGa_{1-x}As$:Mg/GaAs(100) heterostructures

Sample	Energy (wavelength) of transition, eV (nm)
EM2916	1.553 (800)
EM2918	1.563 (795)
EM2921	1.546 (805)

We determine the force constants C_0 and C_1 as

$$C_0 = (3a^3/16)(c_{11} + 2c_{12}),$$
$$C_1 = (a^3/16)(c_{11} - c_{12}). \quad (3)$$

Here, a is the crystal-lattice parameter determined from the high-resolution XRD data and c_{11} and c_{12} are the stress tensor coefficients for the $Al_xGa_{1-x}As$ alloy.

Thus, the LO phonon frequency of the appearing vibrations can be estimated as

$$\omega_{LO}^2 = (8/3\mu d^2)(C_0 + 8C_1), \quad (4)$$

where μ is the reduced mass of vibrating atoms and d is the spacing between them. Since the dopant concentrations in the samples are low, we used the stress tensor coefficients of GaAs [37]. The spacing between nearest neighbors can be calculated with knowledge of the properties of the zinc-blende lattice, in which the $Al_xGa_{1-x}As$ alloy crystallizes.

Calculations in this approximation show that the frequency of the experimentally detected additional mode ($\omega_{LO} = 520$ cm^{-1}) is almost equal to that calculated for Mg–As phonons ($\omega_{LO} = 512$ cm^{-1}). Thus, we can state with confidence that, upon doping, magnesium atoms substitute atoms in the metal sublattice of the $Al_xGa_{1-x}As$ layer, similarly to that already observed in $Al_xGa_{1-x}As$:Si/GaAs(100) and $Al_xGa_{1-x}As$:C/GaAs(100) heterostructures heavily doped with silicon and carbon [8, 9, 11, 32].

When analyzing the Raman spectra, we observe the noticeable redistribution of the intensities of the main and additional phonon modes in the heterostructures (see Fig. 2). Specifically, the LO_{Ga-As} vibration intensity is maximum in the spectrum of sample EM2918, whereas the LO_{Al-As} vibration intensity is maximum in the spectrum of sample EM2916. The additional vibration mode possesses the highest intensity in the spectrum of sample EM2916. By analyzing the relation between the vibration intensities in the spectra and the technological conditions of growth (Table 1), we can draw some conclusions. Magnesium atoms are incorporated in both the metal and nonmetal sublattices of $Al_xGa_{1-x}As$ alloys; in this case, the atomic concentration of magnesium incorporated into all of the $Al_xGa_{1-x}As$ alloys is at a level of 10^{18} cm^{-3}. This concentration can be estimated by analyzing the areas under the main and additional bands, taking into account the fact that the concentration of all atoms in the $Al_xGa_{1-x}As$ alloy is about 10^{22} cm^{-3}.

It is worth noting that the incorporated impurity concentration is low to form an alloy, which is in agreement with the XRD data and the data obtained by us in previous studies. Previously we showed that a significant increase in the Mg atomic concentration yielded enhancement of the intensity of the forbidden main TO phonon vibration mode in the $Al_xGa_{1-x}As$ alloy and a decrease in the intensity of the allowed LO vibration modes related to both Ga–As and Al–As bonds.

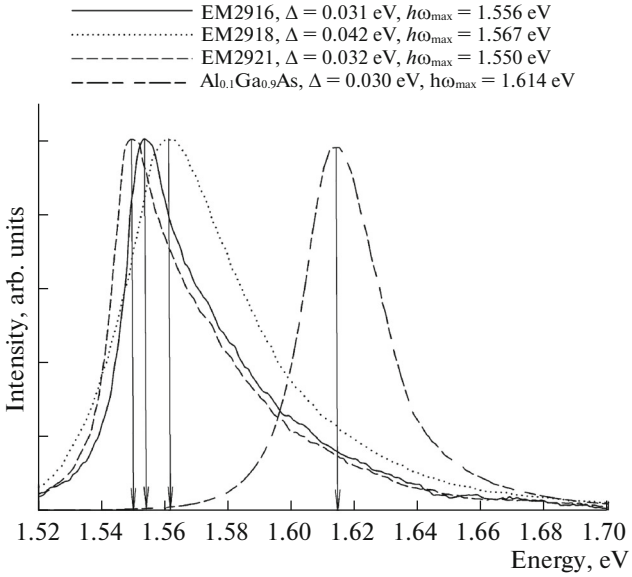

Fig. 3. PL spectra of $Al_xGa_{1-x}As$:Mg/GaAs(100) heterostructures at room temperature.

3.4. PL Spectroscopy

Variations in the conditions of doping, the introduction of impurity atoms in different sublattices and the resultant change in the stoichiometry composition of epitaxial alloys, and the formation of levels in the band gap can be accompanied by the breakage of bonds or by changes in their lengths in the crystal lattice. All of these factors are unavoidably bound to influence changes in the energy characteristics of the material created [9, 38]. Therefore, in addition to the XRD methods and Raman spectroscopy, we here studied the PL spectra. PL spectroscopy is one of the techniques most sensitive to changes in the impurity concentration introduced into the epitaxial layer.

Figure 3 shows the PL spectra of the $Al_xGa_{1-x}As$:Mg/GaAs(100) heterostructures under study. The spectra are recorded at room temperature in the energy range 1.3–2.3 eV typical of emission from $Al_xGa_{1-x}As$ alloy with $x \sim 0.1$. The spectra shown in Fig. 3 are normalized. In addition, Figure 3 shows the spectrum of an undoped $Al_xGa_{1-x}As$ layer with a

similar composition. For the undoped alloy, the emission peak is observed at about 1.614 eV; the half-width of the peak is 0.30 eV. The PL spectra of the $Al_xGa_{1-x}As$:Mg/GaAs(100) heterostructures are identical in shape and observed at longer wavelengths. However, the corresponding shift is no larger than 0.05 eV (Table 3). One more feature of these spectra is a slightly increased half-width of the PL spectra of Mg-doped $Al_xGa_{1-x}As$ layers. In this case, for the heterostructures, we notice some deviation of the spectral band from symmetry in the short-wavelength region.

The observed intense bands are apparently due to different mechanisms of emission in the epitaxial layer (Fig. 3). The major contribution to the observed spectra is made by excitonic PL [39], whose spectral line is the δ function broadened by scattering processes. The high-energy tails in the spectra arise from the annihilation of excitons bound at defects. According to the data of studies in this field, these tails can be attributed to emission from acceptor levels (g–g) and to bound exciton–neutral acceptor transitions (A^0X). Such transitions apparently occur due to an increased acceptor impurity concentration and, correspondingly, density of acceptor states. The data obtained here are in good agreement with the data already obtained in a number of studies of GaAs:Mg samples [22, 23, 27, 28].

Starting from the data of the study [24], in which PL spectroscopy was applied to GaAs samples with different levels of doping with Mg, and comparing these data with the results obtained here, we can state that, in view of the PL-band shape, the number of impurity atoms introduced into the alloy corresponds to the level of doping $\sim 10^{18}$ cm^{-3}. This result agrees with the data obtained by high-resolution XRD and Raman spectroscopy.

4. DISCUSSION

The selection of growth parameters and the simulation of the physical and technological processes of the epitaxial technology on the basis of data of high-resolution XRD, X-ray microanalysis, Hall measurements, and Raman and PL spectroscopies allow us to make a number of inferences about the structural and optical properties of $Al_xGa_{1-x}As$:Mg alloys produced by MOCVD at different Mg-source temperatures.

First, the conditions of growth chosen (the temperature of epitaxy, vapor flows of metal–organic compounds, the carrier gas flow through the dopant impurity (Mg) source) do not change the alloy composition. From the data of studies by structural and spectroscopic methods, it follows that the Mg concentrations introduced into the alloy are supposedly at a level of $\sim 10^{18}$ cm^{-3}. However, depending on the bubbler temperature, not only different concentrations of charge carriers, but also different conductivity types of the epitaxial film are provided. This finding can be easily interpreted, if we take into account the fact that the charge-carrier concentration (determined from Hall measurements) in the film is always the difference between the numbers of acceptors and donors incorporated into the alloy, $N_d - N_a$.

A decrease in the Mg-source temperature to 10°C results not only in a decrease in the impurity mass fraction in the flux, but also in the transition of free Mg atoms into the MgO oxide because of residual oxygen in the carrier gas (hydrogen) and, finally, in the formation of stable Mg-containing complexes in the epitaxial film. All of these factors are favorable for the appearance of a large number of donors in the epitaxial $Al_xGa_{1-x}As$ alloy and for the recompensation of charge carriers, with a change from p-type to n-type conductivity.

An increase in the bubbler temperature to 14°C provides the active incorporation of Mg atoms into the alloy, with substitutions in the metal sublattice, which corresponds to the appearance of an acceptor-type conductivity. A further increase in the bubbler temperature to 18°C yields an increase the Mg atomic concentration in the flux, but at the same time, this increase favors a significant increase in the carbon concentration in the flux. It is well known that, under standard conditions, carbon occupies regular sites of the As sublattice in the crystal lattice of GaAs and GaAs-based ternary compounds and forms shallow acceptor levels. At the same time, it is known that carbon is an amphoteric impurity and can be responsible for conversion of the conductivity type; i.e., in Group-III–V compounds, carbon can be incorporated in the metal sublattice. Taking into account the fact that the activity of Mg atoms is much higher than the activity of carbon, we can reasonably conceive that carbon occupies metal sites in the epitaxial $Al_xGa_{1-x}As$ alloy. This results in a decrease in the number of charge carriers in the films because of impurity recompensation at the same conductivity type.

All of the above-described features influence the PL spectra. From analysis of the results obtained in the study (see Fig. 3), it can be clearly seen that, for different samples, the peak is at different positions in the PL spectra. It is well known that the band gap of the semiconductor decreases, as the dopant density is increased. As a rule, this effect is attributed to narrowing of the band gap or to a red shift. Correlating the data on the technology of growth with PL spectroscopy data and the data of calculation of the band gap of the $Al_{0.103}Ga_{0.897}As$ alloy, we can conclude that the maximum level of doping with impurity atoms is achieved in sample EM921 which was grown at the minimum Mg-source temperature and exhibits n-type conductivity.

5. CONCLUSIONS

By the high-resolution XRD technique and Raman and PL spectroscopies, the structural, optical, and energy properties of epitaxial $Al_xGa_{1-x}As$:Mg/GaAs(100) heterostructures are studied at different levels of doping with Mg. It is shown that, by choosing the technological conditions of production of the $Al_xGa_{1-x}As$:Mg alloy (by varying the dopant-impurity (Mg) source temperature), it is possible to attain not only different conductivity types, but substantially different charge-carrier concentrations in the epitaxial film as well.

ACKNOWLEDGMENTS

We thank V.V. Vasil'eva for her help in preparing the samples for Hall measurements and V.P. Ulina for her participation in discussions of the results.

The study concerned with the development of the technology of the production of epitaxial $Al_xGa_{1-x}As$:Mg layers was supported by the Government order of the Ioffe Physical–Technical Institute; the study concerned with the diagnostics and investigation of the fundamental properties of epitaxial structures was supported by the Ministry of Education and Science of the Russian Federation, Government order for Institutes of Higher Education in the Field of Research Activities 2014 –2016, project no. 740, order no. 3.130.2014/K; the study concerned with the development of methods of controlling the surface morphology and composition and the functional characteristics of low-dimensional systems was supported by the President of the Russian Federation, project no. MK-4865.2016.2.

We acknowledge the Karlsruhe Nano Micro Facility (KNMF, www.kit.edu/knmf) of the Forschungszentrum Karlsruhe for providing access to the equipment of their laboratories.

REFERENCES

1. M. Fehrenbacher, S. Winnerl, H. Schneider, J. Döring, S. C. Kehr, L. M. Eng, Y. Huo, O. G. Schmidt, K. Yao, Y. Liu, and M. Helm, Nano Lett. **15**, 1057 (2015).
2. P. V. Seredin, A. V. Glotov, V. E. Ternovaya, E. P. Domashevskaya, I. N. Arsentiev, L. S. Vavilova, and I. S. Tarasov, Semiconductors **45**, 1433 (2011).
3. K. Yoh and S. Takabayashi, J. Vac. Sci. Technol. B **18**, 1675 (2000).
4. D. Kitchen, A. Richardella, J.-M. Tang, M. E. Flatté, and A. Yazdani, Nature **442**, 436 (2006).
5. F. Münzhuber, T. Kiessling, W. Ossau, L. W. Molenkamp, and G. V. Astakhov, Phys. Rev. B **92**, 115208 (2015).
6. A. J. Ritenour, J. W. Boucher, R. DeLancey, A. L. Greenaway, S. Aloni, and S. W. Boettcher, Energy Env. Sci. **8**, 278 (2015).
7. S. M. Plankina, O. V. Vikhrova, Y. A. Danilov, B. N. Zvonkov, I. L. Kalentyeva, A. V. Nezhdanov, I. I. Chunin, and P. A. Yunin, Semiconductors **49**, 99 (2015).
8. P. V. Seredin, A. V. Glotov, E. P. Domashevskaya, I. N. Arsentiev, D. A. Vinokurov, I. S. Tarasov, and I. A. Zhurbina, Semiconductors **44**, 184 (2010).
9. P. V. Seredin, E. P. Domashevskaya, V. E. Ternovaya, I. N. Arsentyev, D. A. Vinokurov, I. S. Tarasov, and T. Prutskij, Solid State **55**, 2169 (2013).
10. P. V. Seredin, A. V. Glotov, E. P. Domashevskaya, I. N. Arsentyev, D. A. Vinokurov, and I. S. Tarasov, Phys. B: Condens. Matter **405**, 2694 (2010).
11. P. V. Seredin, A. V. Glotov, E. P. Domashevskaya, I. N. Arsentyev, D. A. Vinokurov, and I. S. Tarasov, Phys. B: Condens. Matter **405**, 4607 (2010).
12. K. Uchida, S. Bhunia, N. Sugiyama, M. Furiya, M. Katoh, S. Katoh, S. Nozaki, and H. Morisaki, J. Cryst. Growth **248**, 124 (2003).
13. M. Longo, R. Magnanini, A. Parisini, L. Tarricone, A. Carbognani, C. Bocchi, and E. Gombia, J. Cryst. Growth **248**, 119 (2003).
14. J. Mimila-Arroyo and S. W. Bland, Appl. Phys. Lett. **77**, 1164 (2000).
15. C. Monier, A. G. Baca, S. Z. Sun, E. Armour, F. Newman, and H. Q. Hou, Appl. Phys. Lett. **81**, 2103 (2002).
16. T. Takamoto, T. Agui, E. Ikeda, and H. Kurita, Sol. Energy Mater. Sol. Cells **66**, 511 (2001).
17. P. V. Bulaev, A. A. Marmalyuk, A. A. Padalitsa, D. B. Nikitin, I. D. Zalevsky, V. A. Kapitonov, D. N. Nikolaev, N. A. Pikhtin, A. V. Lyutetskiy, and I. S. Tarasov, J. Cryst. Growth **248**, 114 (2003).
18. P. V. Seredin, A. V. Glotov, E. P. Domashevskaya, I. N. Arsentyev, D. A. Vinokurov, A. L. Stankevich, and I. S. Tarasov, Semiconductors **43**, 1610 (2009).
19. C. L. Reynolds, S. F. Nygren, and C. A. Gaw, Mater. Lett. **4**, 439 (1986).
20. J. Kim, M. S. Kim, D. Y. Kim, H. J. Park, J. S. Kim, D. Y. Lee, J. S. Kim, J. S. Son, H. H. Ryu, G. S. Cho, M. Jeon, and J. Y. Leem, J. Nanosci. Nanotechnol. **9**, 4207 (2009).
21. K. S. Jones, E. L. Allen, H. G. Robinson, D. A. Stevenson, M. D. Deal, and J. D. Plummer, J. Appl. Phys. **70**, 6790 (1991).
22. B. P. Falcão, J. P. Leitão, M. R. Correia, M. R. Soares, F. M. Morales, J. M. Mánuel, R. Garcia, A. Gustafsson, M. V. B. Moreira, A. G. de Oliveira, and J. C. González, J. Appl. Phys. **114**, 183508 (2013).
23. H. Y. Choi, M. Y. Cho, K. G. Yim, M. S. Kim, D.-Y. Lee, J. S. Kim, J. S. Kim, and J.-Y. Leem, Microelectron. Eng. **89**, 6 (2012).
24. J. S. Kim, D. Y. Lee, I. H. Bae, J. I. Lee, S. K. Noh, J. S. Kim, G. H. Kim, S. Ban, S.-K. Kang, S. M. Kim, J. Y. Leem, M. Jeon, and J. S. Son, J. Korean Phys. Soc. **39**, 518 (2001).
25. P. V. Seredin, A. S. Lenshin, A. V. Glotov, I. N. Arsentiev, D. A. Vinokurov, I. S. Tarasov, T. Prutskij,

H. Leiste, and M. Rinke, Semiconductors **48**, 1094 (2014).

26. D. H. Zhang, K. Radhakrishnan, and S. F. Yoon, J. Cryst. Growth **148**, 35 (1995).
27. H. Q. Zheng, K. Radhakrishnan, H. Wang, P. H. Zhang, S. F. Yoon, and G. I. Ng, J. Cryst. Growth **197**, 762 (1999).
28. M. S. Kim, D. Y. Kim, T. H. Kim, G. S. Kim, H. Y. Choi, M. Y. Cho, S. M. Jeon, H. H. Ryu, W. W. Park, J. Y. Leem, J. S. Kim, J. S. Kim, D. Y. Lee, and J. S. Son, J. Korean Phys. Soc. **54**, 673 (2009).
29. J. Xu, E. Towe, Q. Yuan, and R. Hull, J. Cryst. Growth **196**, 26 (1999).
30. A. P. V. Seredin, A. V. Glotov, A. S. Lenshin, I. N. Arsentiev, D. A. Vinokurov, T. Prutskij, H. Leiste, and M. Rinke, Semiconductors **48**, 21 (2014).
31. V. I. Punegov, Phys. Usp. **58**, 419 (2015).
32. P. V. Seredin, A. V. Glotov, V. E. Ternovaya, E. P. Domashevskaya, I. N. Arsentiev, D. A. Vinokurov, A. L. Stankevich, and I. S. Tarasov, Semiconductors **45**, 481 (2011).
33. P. V. Seredin, A. V. Glotov, E. P. Domashevskaya, A. S. Lenshin, M. S. Smirnov, I. N. Arsentiev, D. A. Vinokurov, A. L. Stankevich, and I. S. Tarasov, Semiconductors **46**, 719 (2012).
34. W. Hayes and R. Loudon, *Scattering of Light by Crystals* (Wiley, New York, 1978).
35. W. A. Harrison, *Electronic Structure and the Properties of Solids: The Physics of the Chemical Bond* (Dover, New York, 1989).
36. D. Wolverson, D. M. Bird, C. Bradford, K. A. Prior, and B. C. Cavenett, Phys. Rev. B **64**, 113203 (2001).
37. M. E. Levinshtein, S. L. Rumyantsev, and M. Shur, *Handbook Series on Semiconductor Parameters* (World Scientific, Singapore, 1999), Vol. 2.
38. P. V. Seredin, A. V. Glotov, E. P. Domashevskaya, I. N. Arsentyev, D. A. Vinokurov, and I. S. Tarasov, Appl. Surf. Sci. **267**, 181 (2013).
39. A. P. Levanyuk and V. V. Osipov, Sov. Phys. Usp. **24**, 187 (1981).

Translated by E. Smorgonskaya